Filament structure of bacterial tubulin homologue TubZ

Christopher H. S. Aylett, Qing Wang, Katharine A. Michie, Linda A. Amos, and Jan Löwe[1]

Medical Research Council Laboratory of Molecular Biology, Cambridge CB2 0QH, United Kingdom

Edited by Stephen C. Harrison, Harvard Medical School, Boston, MA, and approved September 24, 2010 (received for review July 13, 2010)

Low copy number plasmids often depend on accurate partitioning systems for their continued survival. Generally, such systems consist of a centromere-like region of DNA, a DNA-binding adaptor, and a polymerizing cytomotive filament. Together these components drive newly replicated plasmids to opposite ends of the dividing cell. The *Bacillus thuringiensis* plasmid pBToxis relies on a filament of the tubulin/FtsZ-like protein TubZ for its segregation. By combining crystallography and electron microscopy, we have determined the structure of this filament. We explain how GTP hydrolysis weakens the subunit–subunit contact and also shed light on the partitioning of the plasmid–adaptor complex. The double helical superstructure of TubZ filaments is unusual for tubulin-like proteins. Filaments of ParM, the actin-like partitioning protein, are also double helical. We suggest that convergent evolution shapes these different types of cytomotive filaments toward a general mechanism for plasmid separation.

DNA segregation | plasmid partitioning | RepX

For a plasmid to be inherited, it must be replicated and then partitioned to both daughter cells. In eukaryotes, partitioning of replicated chromosomes is carried out by the tubulin cytoskeleton, which separates regions of centromeric DNA. Microtubules are linked to DNA by the kinetochore, which functions as an adaptor. The prokaryotic plasmid partitioning systems so far uncovered are arranged similarly; an adaptor protein links a centromere-like region of DNA and a nucleotide-hydrolyzing protein required for movement (1, 2). However, all known plasmid partitioning systems are minimalist, each component consisting of a single protein. On the basis of the nature of the protein that is responsible for movement, plasmid partitioning systems have been named type I, II, and III (3, 4), types II and III having filament-forming cytoskeletal proteins of the actin and tubulin type at their core. No cytoskeletal motor proteins such as myosin, kinesin, or dynein are known in prokaryotes, and, in partitioning systems, the filament dynamics themselves are responsible for movement. Because the filaments generate force alone, filament-forming proteins that utilize nucleotide turnover to regulate polymerization are "cytomotive" (5).

Plasmid partitioning systems based on Walker ATPases [ParA-like, type I (6)] and actin-like ATPases [ParM-like, type II (1, 7)] have been known for some time. More recently, tubulin/FtsZ-like GTPases [TubZ-like, type III (4, 8, 9)] have been discovered in partitioning systems. Type III systems were first found in *Bacillus anthracis* (9, 10); however, the best-characterized example is from *Bacillus thuringiensis*. Plasmid pBtoxis (11) relies on the TubZR*C* partitioning system for its stability (4, 12). A DNA centromere, *tubC*, is bound by the adaptor protein TubR (7), which in turn is thought to recruit TubZ. TubZ then forms a cytomotive filament to drive the plasmid to the cell pole. The C terminus of TubZ has been implicated in binding TubR, although the specific binding site remains unknown (13).

TubZ and other type III plasmid partitioning proteins polymerize and have been shown to share properties with tubulin. Like tubulin they require a relatively high critical concentration for assembly, hydrolyze GTP quickly, form filaments containing predominantly GDP, and presumably therefore have a GTP cap (10, 14, 15). In filaments of FtsZ, the tubulin homologue that mediates bacterial cytokinesis, many subunits contain GTP (16). Tubulin and ParM are believed to undergo dynamic instability whereby the filaments depolymerize from both ends once the NTP cap that stabilizes the ends has been lost. In contrast, TubZ filaments treadmill (polymerizing at one end while depolymerizing at the other), bundle together, and are somewhat flexible (4, 10). These traits are more similar to actin filaments (5). The structure of TubZ has recently been solved in its monomeric state by using X-ray crystallography (13), confirming that it indeed belongs to the tubulin/FtsZ family of proteins.

Here we present crystal structures of both GTPγS and GDP-bound protofilaments of TubZ and helical reconstructions from electron microscopy of negatively stained filaments in vitro. The crystal structures reveal the active site in both of the states known to occur in filaments and allow us to explain the loss of subunit–subunit affinity upon nucleotide hydrolysis. Electron microscopy shows that TubZ forms a parallel, double helical filament both in vitro and in cells. By combining these structures we have produced a pseudoatomic model of the TubZ filament. The superstructure of the helix is reminiscent of that formed by the actin-like partitioning protein ParM (17), suggesting convergent evolution toward a general method of plasmid partitioning by a double helical cytomotive filament.

Results and Discussion

Crystal Structures of the TubZ Protofilament. We cloned and overproduced TubZ from *B. thuringiensis*. Full-length TubZ did not crystallize; however, FtsZ homologues had required truncation of unstructured regions of the protein to crystallize previously (18), so we defined a minimal and stable construct encompassing residues 1–421 of TubZ (TubZ1-421) by limited proteolysis and sequence analysis (Figs. S1 and S2) and purified it to homogeneity by chromatography (Fig. 1*A*).

TubZ1-421 crystallized as a continuous protofilament. We solved separate crystal forms containing GTPγS (R/R_{free}, 0.23/0.28) and GDP (R/R_{free}, 0.23/0.29). The resolution was limited to 3 Å because of the size of the unit cell (Fig. S3). Our structures comprise 7 GTPγS-bound subunits in one form and 11 GDP and 1 aposubunit in the other (Table S1).

TubZ Is Homologous to Tubulin and FtsZ. As was determined previously for TubZ in a monomeric form (13), the fold of TubZ

Author contributions: C.H.S.A. and J.L. designed research; C.H.S.A., Q.W., K.A.M., L.A.A., and J.L. performed research; C.H.S.A., L.A.A., and J.L. analyzed data; and C.H.S.A. and J.L. wrote the paper.

The authors declare no conflict of interest.

This article is a PNAS Direct Submission.

Data deposition: The atomic coordinates and structure factor amplitudes for TubZ GTPγS and GDP have been deposited in the Protein Data Bank, www.pdb.org (PDB ID codes 2XKA and 2XKB). The electron microscopy densities for TubZ double, quadruple, Trx double, and GFP double filaments have been deposited with the Electron Microscopy Data Bank as EMDB ID codes 1757, 1758, 1759, and 1760.

[1]To whom correspondence should be addressed. E-mail: jyl@mrc-lmb.cam.ac.uk.

This article contains supporting information online at www.pnas.org/lookup/suppl/doi:10.1073/pnas.1010176107/-/DCSupplemental.

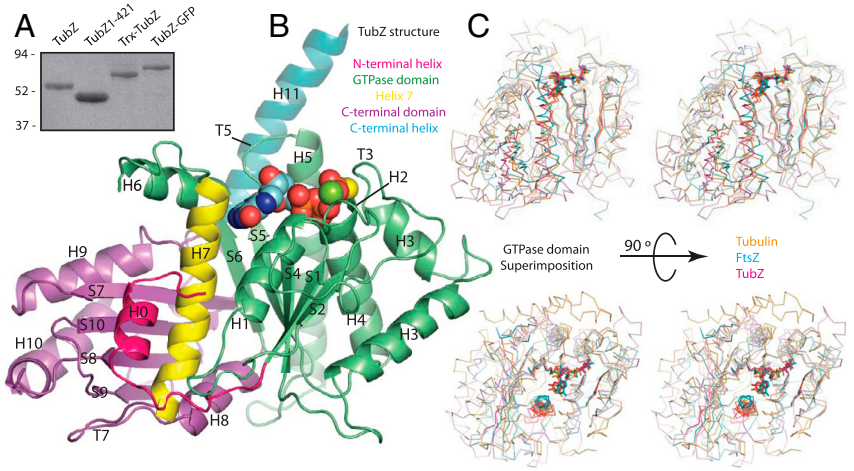

Fig. 1. TubZ is a member of the tubulin/FtsZ family. (*A*) SDS-PAGE of purified TubZ proteins. TubZ: full-length TubZ with a C-terminal hexahistidine tag; TubZ1-421: TubZ (L2V in this protein only) truncated C-terminally at residue 421 and untagged; Trx-TubZ: N-terminal thioredoxin fusion to full-length TubZ with a C-terminal hexahistidine tag; TubZ-GFP: hexahistidine tagged C-terminal fusion of TubZ to GFP molecular mass in kDa. (*B*) Cartoon representation of TubZ1-421•GTPγS; chain D. Secondary structural elements are labeled according to (21). The N-terminal extension is pink, the GTPase domain green, helix 7 yellow, the C-terminal domain purple, and the C-terminal tail blue. (*C*) Stereoscopic Cα traces of bovine tubulin (orange) [Protein Data Bank (PDB) ID code 1JFF), *M. jannaschii* FtsZ (blue) (PDB ID code 1W5A), and TubZ1-421 (pink) superimposed using only the GTPase domain. The β-sheets, H7, and nucleotide are highlighted in the same color. The lower pair have been rotated by 90°.

places it within the tubulin/FtsZ family, despite very low sequence similarity to these proteins (~15%). The evolutionarily conserved tubulin/FtsZ fold consists of an N-terminal GTPase domain and a C-terminal domain, shown in Fig. 1*B*. TubZ possesses an additional helical C-terminal tail, which is conformationally flexible.

The GTPase domains of *Methanococcus jannaschii* FtsZ (19) and bovine α-tubulin (20) superimpose well with TubZ, whereas their C-terminal domains are a little more divergent. The relative orientations of the TubZ GTPase and C-terminal domains are different from those in FtsZ and tubulin (Fig. 1*C*). In TubZ the C-terminal domain is rotated and tilted outward relative to the GTPase domain rather than nestling under it. This rotation begins in H7, and the space between the domains in TubZ is filled by H0 and the loop following it (Fig. 1*B*). The changed position of the two domains reflects evolutionary adaptation to a task with different demands from those faced by either FtsZ or tubulin.

The TubZ Active Site and Interface Is Close to That of Tubulin. Our crystal structures reveal the active site in GTPγS, GDP, and apostates. The TubZ active site residues are conserved from both tubulin and FtsZ. Furthermore, the subunit–subunit interaction is close to the α/β–tubulin interface (Fig. 2*B*). The interaction in the only dimeric FtsZ structure (19) is different (Fig. 2*B*); however, we suspect that this FtsZ dimer may be distorted because of the crystal lattice and that the interface contacts are essential parts of the active site.

The C-terminal domain of the adjacent subunit interacts with the GTPase domain, loop T7 (20) protruding into the active site cleft, placing the base of H8 over the γ-phosphate (Fig. 2*B* and Fig. S4). Formation of the GTPase active site couples polymerization to hydrolysis. Conserved aspartates 266 and 269 and lysine 359 are contributed by the C-terminal domain of the adjacent subunit, whereas the GTPase domain coordinates the essential Mg^{2+} ion, through aspartate 64 in most of the GTPγS-bound subunits, and forms the nucleotide binding site (Fig. 2*C*).

Nucleotide exchange appears to be difficult in the protofilament, requiring the outward movement of large regions, as is the case in tubulin. On the other hand, phosphate release after hydrolysis may occur through a channel emerging from the active site above the C-terminal domain, which is much wider in TubZ than in tubulin and may suggest faster release of the phosphate (Fig. S4). Release changes the active site substantially.

The Subunit–Subunit Interface Is Destabilized by the Release of Mg^{2+} and Phosphate. Although no conformational changes were seen in monomeric TubZ between the apo- and GTPγS states (13), we believe that this is an artifact because the nucleotide was soaked into existing crystals. Whereas the protein's fold remains the same in the polymer as in the monomer, our GTPγS, GDP, and apoforms are substantially different, and the TubZ intersubunit interface is destabilized in the GDP and apostates.

In the absence of the γ-phosphate, two sections of the active site relax to alternate conformations. Loop T3, which contacts H8 in the adjacent subunit, becomes completely disordered, whereas density for H3 becomes poor, supporting the observations of Díaz et al. in FtsZ (22). Although the loop displays two conformations in the GTPγS state, the tip of the loop is arginine 87, which contacts the γ-phosphate in both conformations. All GTPγS-bound subunits also retain a Mg^{2+} ion although only four of 11 GDP-bound subunits do so, despite crystallization with 200 mM $MgCl_2$. When aspartate 64 in H2 is not coordinated to the Mg^{2+} ion, this helix rolls away from the active site (Fig. 2*C* and Fig. S5). Given that this region interacts with loop T7, which also contacts the Mg^{2+} ion, this change weakens the interaction between subunits. These changes link hydrolysis to destabilization of the intersubunit interface, which is essential for the filament to treadmill.

The Rotated C-Terminal Domain Twists the TubZ Filament. All our TubZ protofilaments show right-handed twist (Fig. 2*A*). The GTPγS protofilament turns 360° over 14 subunits, whereas both GDP filaments repeat in 12. Both tubulin and FtsZ have no twist (Fig. 2*B*). Surprisingly, the intersubunit interaction is conserved between tubulin and TubZ (Fig. 2*B* and Fig. S4), exhibiting little relative rotation, and contacts in the same regions (Fig. S6). It is the relative rotation between the C-terminal domain and GTPase domain within the subunit that gives rise to twist in the TubZ protofilament.

The result is that the vector of protofilament polymerization in TubZ is different from that in both tubulin and FtsZ. The large protrusion of the TubZ GTPase domain is because of this change (Fig. 2*A*). Compared to tubulin, the TubZ C-terminal domain is rotated outward, away from the GTPase domain, as well as being rotated around the axis along which tubulin polymerizes (Fig. 1*C* and Fig. S6), making the direction of TubZ protofilament formation and the axis of rotation between the two domains of the subunit colinear. Without the change in the vector of polymerization, the writhe of the protofilament would increase around the center of rotation, near the C terminus of the subunit.

The writhe of the protofilaments is, in fact, generated by the tilt of adjacent TubZ subunits relative to those in tubulin (Fig. 2*B* and Fig. S6). They tilt from the C terminus toward the N terminus, the base of the subunit contacting the C-terminal tail of the adjacent subunit. The reason for these differences in TubZ to generate twist and writhe became apparent as soon as we looked at filaments assembled in solution.

TubZ Forms Single, Double, and Quadruple Filaments in Vitro. When we observed polymerized TubZ by negative stain electron micro-

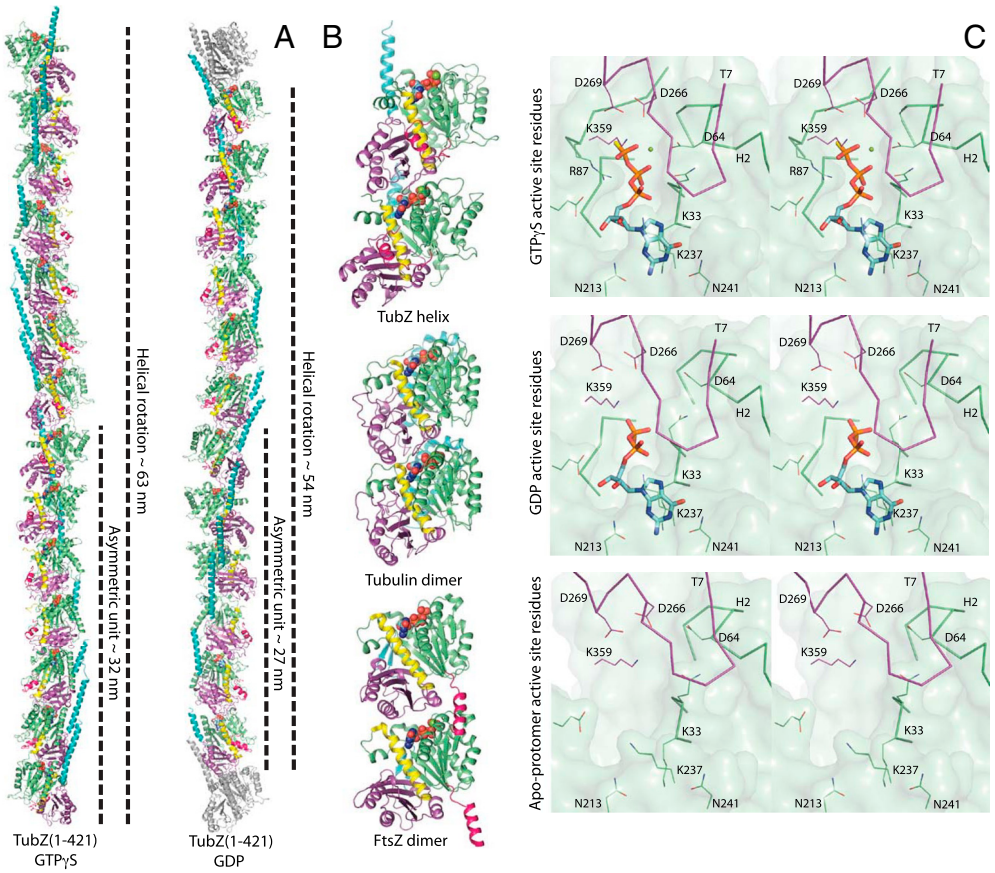

Fig. 2. Structure of the TubZ protofilament. (*A*) Protofilaments from the TubZ1-421•GTPγS and GDP crystal forms. Both crystal forms contain continuous protofilaments with 14 and 12 subunits per complete turn, respectively. The lengths of the unit cell and asymmetric unit are indicated. The color scheme is identical to Fig. 1*B*, excluding two gray monomers corresponding to the first subunits of the next unit cell in the GDP form. (*B*) Cartoons of the protofilament dimers of bovine tubulin (PDB ID code 1JFF), *M. jannaschii* FtsZ (PDB ID code 1W5A), and TubZ (this study, TubZ1-421•GTPγS chains D and E). In each case, the lower monomer was superimposed by using the GTPase domain alone. All subunits are colored as in Fig. 1*B*. (*C*) Stereoscopic representations of the TubZ active site in Mg^{2+}•GTPγS, GDP, and apostates. Interacting residues and regions of backbone are shown as skeleton and Cα traces, respectively. The most representative interfaces have been selected for Mg^{2+}•GTPγS and GDP states for clarity—see Fig. S5 for a superposition of all interfaces. The GTPase domain is green, the C-terminal domain purple, and the nucleotide blue.

scopy, we found large bundles of filaments. The filaments were usually relatively straight, and bundles of filaments often covered distances of over 10 μm. The long filaments that separated from the bundles were formed by two protofilaments rotating around a shared axis, with cross-overs at ~35 nm (Fig. 3 *C*–*E*). We also found wider filaments with less clear cross-overs at ~25 nm (Fig. 3 *A*, *B*, and *F*). These proved difficult to categorize; however, we eventually found clear conjunctions of double filaments in the process of forming larger filaments, implying quadruple protofilaments (Fig. 3*A*, marked with *).

The clear intertwining of the protofilaments explains why TubZ protofilaments must twist and writhe: to place the same surface of each subunit on the interface between two protofilaments and to wrap around one another without clashing, producing double helical filaments with closed symmetry. The identification of quadruple as well as double filaments posed a new question, however: Which filament is present in cells?

TubZ Forms Double Filaments in Cells Overexpressing TubZ. We used electron cryomicroscopy to image snap-frozen *Escherichia coli* cells overexpressing full-length TubZ. Tomographic reconstruction of these cells revealed large, well-ordered bundles of straight filaments in the cytoplasm (Fig. 3*H*). Filaments in the bundles appeared to have some density between them, raising the possibility that the C-terminal tail of TubZ mediates bundling. The individual filaments were similar in morphology to those observed for TubZ in vitro (Fig. 3*H*). Fourier transforms of filaments in tomograms produced layer lines corresponding to a helical pitch of ~35 nm, consistent with double filaments (Fig. 3*I*).

Further support for the double filament as the basic unit in cells was gained from cryosections transecting the bundles (Fig. 3*J*); the filaments were seen to be ~7 nm in diameter spaced on an approximately square lattice of ~10 nm. The diameters measured from negatively stained TubZ filaments in vitro were ~8 nm for double filaments and ~10 nm for quadruple filaments. The wider quadruple filaments would need to be close-packed on the observed lattice, with no space between them, to fit the observed spacing. Furthermore, no central cavities within filaments were observed in filaments formed in cells. Such cavities would be expected for quadruple filaments given that they are formed by two interwound helical ribbons of TubZ protofilaments (Fig. S7*B*).

TubZ Double Filaments Are Parallel and Right-Handed and Rotate over ~17 Subunits. To determine the handedness of the filaments, we used rotary shadowing to visualize them in vitro. With the viewing direction directly confirmed by an asymmetric finder grid, the EM images indicated that TubZ filaments were right-handed (Fig. 3*G*). Fittingly, this is the same hand as TubZ protofilaments in the crystal structures (Fig. 2*A*).

Fourier transformation of filaments in negative stain gave clear layer lines that we indexed by using a helical lattice (Fig. 4*A*). Double filaments always gave one or two strong layer lines from the gyres at spacings corresponding to the interval between cross-overs. The best Fourier transforms also had meridional and near-meridional layer lines corresponding to spacings of 3.5–5.5 nm. The spacing of the meridional layer line for the subunit rise was roughly 8.5-fold the spacing of the first layer line from the gyres, indicating that roughly 17 subunits will make up one turn, several more than in the protofilaments in the crystal structures (Figs. 4*A* and 2*A*). This change can be accounted for by increased writhe, which is necessary to cover the greater distance around the other protofilament.

Helical Reconstructions from EM Data Can Be Fitted with the Crystallographic Protofilament. We reconstructed the TubZ double filament in three dimensions from the electron microscopy helical lattice and then fitted the average of the five best densities with

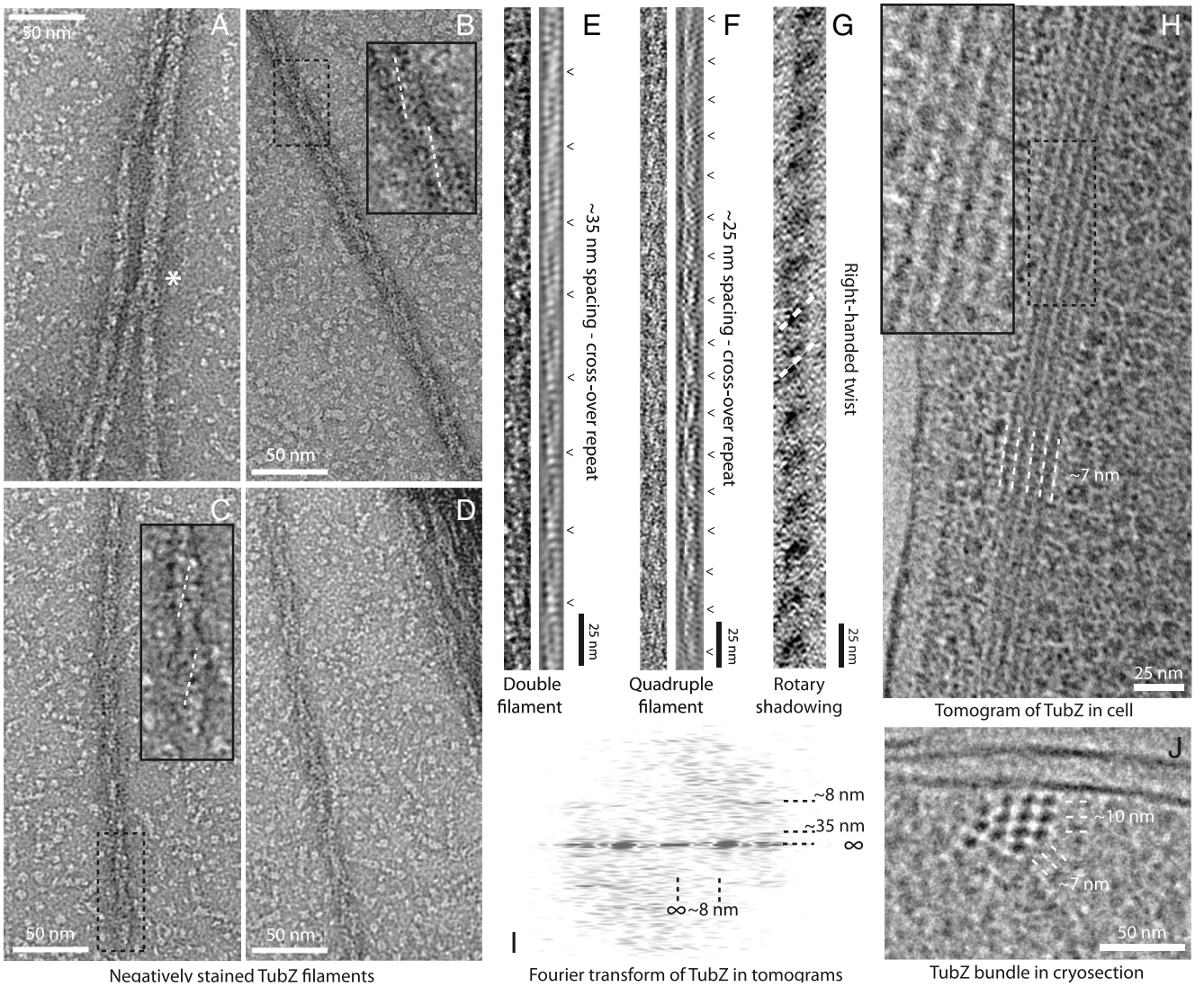

Fig. 3. TubZ forms filaments both in vitro and when overexpressed in *E. coli*. (*A*–*D*) Negatively stained electron micrographs of TubZ filaments assembled in vitro, with magnified insets. Two double filaments join to form a quadruple in *A*, marked with *, whereas *B* represents a quadruple and *C* and *D* double filaments of TubZ. Gyre lines are marked in white. (*E* and *F*) Pairs of straightened and filtered TubZ filaments. The filament in *E* is double and in *F* quadruple. The crossovers are annotated alongside. (*G*) A rotary shadowed TubZ filament as viewed from above. Right-handed gyres are indicated. (*H*) Slice through a tomogram of plunge-frozen *E. coli* cells overexpressing full-length TubZ. Filaments are visible as a bundle, magnified in the inset. The filament lateral spacing at this angle is shown. (*I*) Fourier transform of the bundles of TubZ filaments in the tomograms. The lateral and significant longitudinal spacings, including the ~35 nm cross-over repeat, are annotated. (*J*) A 50 nm cryosection through plunge-frozen *E. coli* cells expressing TubZ. A cross-section through a bundle of filaments is visible, looking along the filaments. Lateral spacings in two different directions are annotated and suggest double helices.

the structure of the GTPγS protofilament. Taking into account the writhe of the protofilament from the crystal and the strong surface striations leaves only one possible orientation (Fig. 4*B*). The writhe of the crystal protofilaments does not match the reconstruction exactly, and the ends of the asymmetric unit protrude slightly as the error accumulates, but otherwise the fit is surprisingly good. The GTPase domain creates a large protrusion on the back of the TubZ filament, characterizing one side of the crystal structure. The density from electron microscopy also shows a protrusion on one side. The resulting fit places the N terminus of TubZ near the interprotofilament interface and the C terminus outside of the double filament (Fig. 4*B*). A model from the fit using helical symmetry reconstitutes an active site and interface essentially identical to the crystal structure (Fig. 4*C*).

Fusion Protein Reconstructions Confirm That the N Terminus Is Inside and the C Terminus Outside. To independently confirm our model for the orientation of TubZ, we fused domains to the termini of TubZ. In separate constructs, thioredoxin was fused N-terminally (Trx-TubZ) and green fluorescent protein C-terminally (TubZ-GFP) (Fig. S3). Trx-TubZ did not initially polymerize, which was not unexpected given the predicted position of the N terminus. We managed to polymerize Trx-TubZ in the presence of DEAE-dextran, however, whereas TubZ-GFP polymerized readily. Both formed filaments similar to those of native TubZ.

We then reconstructed the new filaments in three dimensions to reveal the location of the labels. In agreement with the fit into the native map, extra density for thioredoxin was present near the cleft marking the protofilament interface (Fig. 4*B*, marked †), suggesting that it had been blocking the interaction of the protofilaments in agreement with the fit into the native map. This contact is occupied by the N-terminal loop of both TubZ subunits, indicating a further function for this extension as well as its role in reshaping the angle between the GTPase domain and the C-terminal domain (Fig. 4 *B* and *C*).

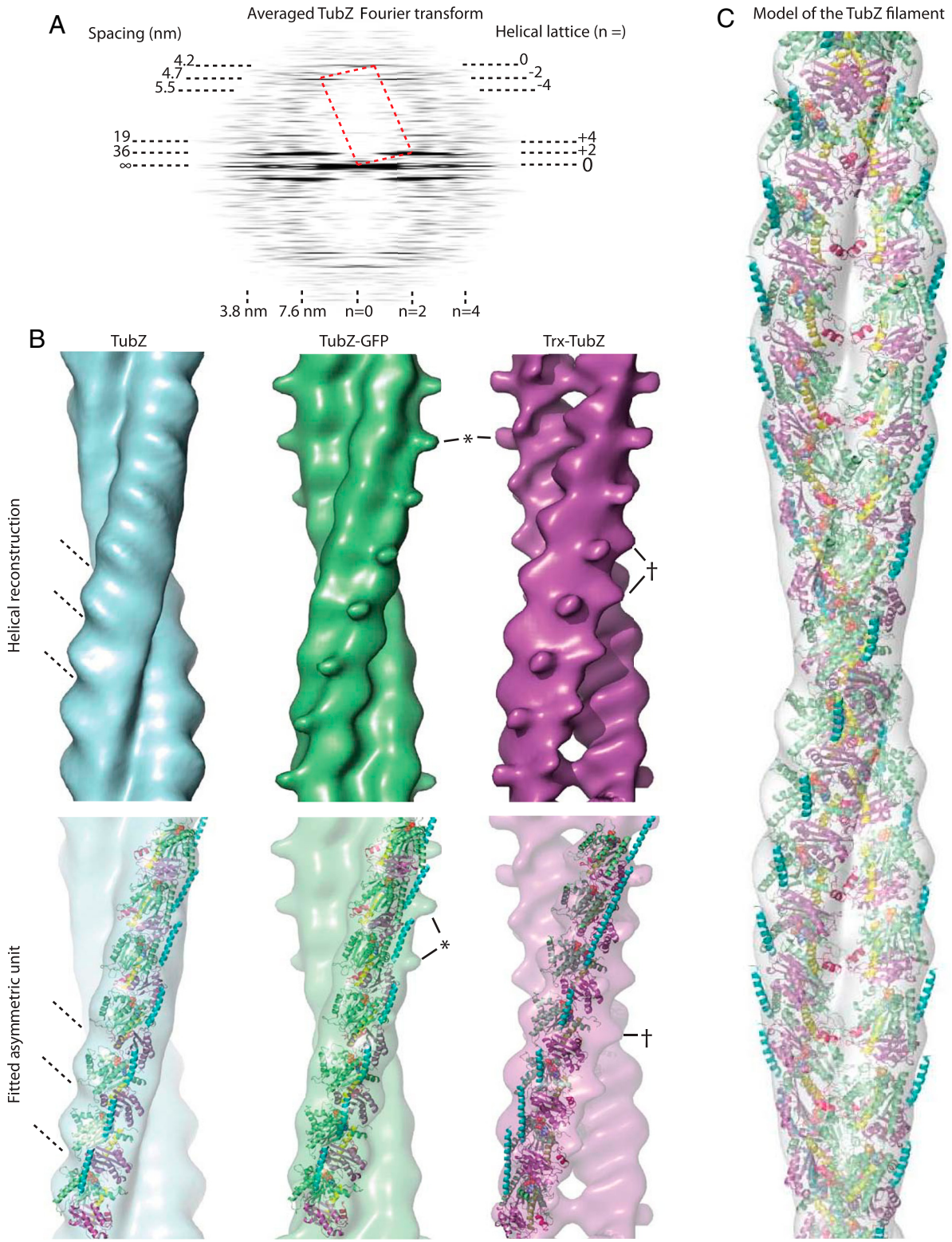

Fig. 4. Structure of TubZ double helical filaments. (*A*) Averaged Fourier transform of straightened TubZ filaments showing the helical lattice and its latitudinal and longitudinal spacings (nanometers). The reciprocal unit cell is shown in red dotted lines. (*B*) Surface map (*Upper*) and fit (*Lower*) of the GTPγS asymmetric unit into each of the TubZ filament maps. The tilt of the subunits and the reconstructed density is indicated. The protrusion adjacent the C terminus is marked (*), as is the extra density adjacent the N terminus and the protofilament interface (†). Native TubZ is blue, Trx-TubZ purple, and TubZ-GFP green. Note that for this fit and figure the crystal structure of the protofilament has not been adjusted in any way. The writhe of the crystal structure protofilament indicates the correct orientation, as do the positions of the extra densities generated by thioredoxin and GFP. (*C*) Cartoon and surface representation of the final, adjusted, and fitted TubZ model (42 Å rise and 21° twist per subunit). A double helical filament restricts growth to one dimension, and it is presumed that TubZ represents a special adaptation of the tubulin/ftsZ family to yield filaments that superficially resemble F-actin and ParM through convergent evolution.

The reconstruction of TubZ-GFP filaments did not immediately reveal extra density. The densities of several filaments consistently produced a protrusion next to the fitted C terminus (Fig. 4*B*, marked *), which had been noted in some individual wild-type reconstructions but which had not been retained after averaging of the five best densities. TubZ-GFP filaments consistently demonstrated this feature. It seems most likely that the C terminus can easily separate from the side of the filament and protrudes flexibly more frequently in TubZ-GFP because of the added domain. GFP is therefore not itself resolved, because it will not be ordered relative to the filament. The density seen is from the C-terminal tail, helping to confirm the position of the C terminus, which has been implicated in binding to the adaptor complex (13), on the exterior where an interaction would occur (Fig. 4 *B* and *C*).

TubZ as a Partitioning Protein. TubZ represents an adaptation of the tubulin/FtsZ family cytoskeletal filament to an unusual role for such proteins. Significant differences in the structure of the protein create twist and writhe, characteristics absent from tubulin and FtsZ filaments. Although the active site and interface are conserved from tubulin, the relationship between the domains is different, inducing the twist of the protofilament. The more conserved feature of the filament in evolutionary terms appears to be the interaction of the GTPase domain and the C-terminal domain between subunits, not within them. This observation makes sense given that the constraints on the GTPase reaction and filament formation are great, because a small molecule is involved, whereas small changes in angle between domains within the protein may be tolerated with ease.

Clearly, for such changes to evolve, the function of TubZ must favor the double helical filaments they generate. Whereas tubulin performs a DNA partitioning function in eukaryotes, it is generally depolymerization and motor proteins that provide the motive force. Tubulin microtubules consist of 13 protofilaments, which provide a large binding surface for motor proteins and rigidity to haul chromosomes across the cell. On the other hand, we have shown that TubZ filaments have a simple twofold rotational symmetry. Presumably, these cytomotive filaments must push plasmids from replication sites in the nucleoid to the cell pole.

The TubZ filament is structurally reminiscent of ParM, the prototypical actin-like partitioning filament, which also forms twisted, double filaments. TubZ and ParM both form long straight filaments in the cell and can bundle (23). It is striking that two such disparate proteins have evolved to produce similar superstructures for a similar purpose, and this convergence suggests strong evolutionary constraints on partitioning systems.

A two-stranded filament is more stable than a single protofilament but has closed rotational symmetry, naturally restricting growth to one dimension. It seems natural that this simple architecture minimizes the subunits required for each filament and thus the energy used, which is obviously of benefit to a partitioning system, which must avoid being overly detrimental to the plasmid's host. Bundling allows lateral stabilization of the filaments and possibly movement of multiple plasmids together. The fact that filaments are relatively straight will also ensure that the plasmids are carried to the end of a rod-shaped cell. If the persistence length is sufficient, clashes with the plasma membrane as the filament extends will naturally guide it to the cell poles.

Materials and Methods

Detailed methods are provided in *SI Materials and Methods*. Briefly, TubZ proteins were expressed in *E. coli* and purified, TubZ was crystallized with GTPγS and GDP in the presence of PEG and $MgCl_2$, and the structures were solved by using Se single anomalous dispersion and molecular replacement. Filaments for in-cell electron microscopy were expressed in *E. coli* and resolved by using cryosectioning or electron cryotomography. Filaments for in vitro electron microscopy were polymerized at pH 7.5 by using GTPγS and stained with uranyl acetate. Fourier transforms of single filaments were indexed, reconstructed in three dimensions, and fitted with the crystallographic protofilaments.

ACKNOWLEDGMENTS. We thank Rachel Larsen and Joseph Pogliano (University of California San Diego) for providing the TubZ gene, Fabrice Gorrec at our crystallization facility, Chen Shaoxia at our EM facility, and Sonja Dunbar for summer work. We acknowledge the European Synchrotron Radiation Facility and Diamond Light Source for providing excellent service and support. Q.W. acknowledges receipt of a Dorothy Hodgkin award from Cambridge University Overseas Trust.

1. Pogliano J (2004) DNA segregation by bacterial actin homologs. *Dev Cell* 6:3–4.
2. Salje J (2010) Plasmid segregation: How to survive as an extra piece of DNA. *Crit Rev Biochem Mol Biol* 45:296–317.
3. Gerdes K, Møller-Jensen J, Bugge Jensen R (2000) Plasmid and chromosome partitioning: Surprises from phylogeny. *Mol Microbiol* 37:455–466.
4. Larsen RA, et al. (2007) Treadmilling of a prokaryotic tubulin-like protein, TubZ, required for plasmid stability in *Bacillus thuringiensis*. *Gene Dev* 21:1340–1352.
5. Löwe J, Amos LA (2009) Evolution of cytomotive filaments: The cytoskeleton from prokaryotes to eukaryotes. *Int J Biochem Cell Biol* 41:323–329.
6. Abeles AL, Friedman SA, Austin SJ (1985) Partition of unit-copy miniplasmids to daughter cells III. The DNA sequence and functional organization of the P1 partition region. *J Mol Biol* 185:261–272.
7. Salje J, Löwe J (2008) Bacterial actin: Architecture of the ParMRC plasmid DNA partitioning complex. *EMBO J* 27:2230–2238.
8. Tang M, Bideshi DK, Park HW, Federici BA (2007) Iteron-binding ORF157 and FtsZ-like ORF156 proteins encoded by pBtoxis play a role in its replication in *Bacillus thuringiensis subsp. israelensis*. *J Bacteriol* 189:8053–8058.
9. Tinsley E, Khan SA (2006) A novel FtsZ-like protein is involved in replication of the Anthrax toxin-encoding pXO1 plasmid in *Bacillus anthracis*. *J Bacteriol* 188:2829–2835.
10. Anand SP, Akhtar P, Tinsley E, Watkins SC, Khan SA (2008) GTP-dependent polymerization of the tubulin-like RepX replication protein encoded by the pXO1 plasmid of *Bacillus anthracis*. *Mol Microbiol* 67:881–890.
11. Berry C, et al. (2002) Complete sequence and organization of pBtoxis, the toxin-coding plasmid of *Bacillus thuringiensis subsp. israelensis*. *Appl Environ Microbiol* 68:5082–5095.
12. Tang M, Bideshi DK, Park HW, Federici BA (2006) Minireplicon from pBtoxis of *Bacillus thuringiensis subsp. israelensis*. *Appl Environ Microbiol* 72:6948–6954.
13. Ni L, Xu W, Kumaraswami M, Schumacher MA (2010) Plasmid protein TubR uses a distinct mode of HTH-DNA binding and recruits the prokaryotic tubulin homolog TubZ to effect DNA partition. *Proc Natl Acad Sci USA* 107:11763–11768.
14. Chen Y, Erickson HP (2008) In vitro assembly studies of FtsZ/tubulin-like proteins (TubZ) from *Bacillus* plasmids: Evidence for a capping mechanism. *J Biol Chem* 283:8102–8109.
15. Akhtar P, Anand SP, Watkins SC, Khan SA (2009) The tubulin-like RepX protein encoded by the pXO1 plasmid forms polymers in vivo in *Bacillus anthracis*. *J Bacteriol* 191:2493–2500.
16. Chen Y, Erickson HP (2009) FtsZ filament dynamics at steady state: Subunit exchange with and without nucleotide hydrolysis. *Biochemistry* 48:6664–6673.
17. van den Ent F, Møller-Jensen J, Amos LA, Gerdes K, Löwe J (2002) F-actin-like filaments formed by plasmid segregation protein ParM. *EMBO J* 21:6935–6943.
18. Oliva MA, Trambaiolo D, Löwe J (2007) Structural insights into the conformational variability of FtsZ. *J Mol Biol* 373:1229–1242.
19. Oliva MA, Cordell SC, Löwe J (2004) Structural insights into FtsZ protofilament formation. *Nat Struct Mol Biol* 11:1243–1250.
20. Löwe J, Li H, Downing KH, Nogales E (2001) Refined structure of alpha beta-tubulin at 3.5 Å resolution. *J Mol Biol* 313:1045–1057.
21. Nogales E, Downing KH, Amos LA, Löwe J (1998) Tubulin and FtsZ form a distinct family of GTPases. *Nat Struct Biol* 5:451–458.
22. Díaz JF, et al. (2001) Activation of cell division protein FtsZ. Control of switch loop T3 conformation by the nucleotide gamma-phosphate. *J Biol Chem* 276:17307–17315.
23. Salje J, Zuber B, Löwe J (2009) Electron cryomicroscopy of *E. coli* reveals filament bundles involved in plasmid DNA segregation. *Science* 323(5913):509–512.